

## Reusable Heterogeneous SnO<sub>2</sub>/ZnO Catalyst for Biodiesel Production from Acidified/Acid Oils

Daiane F. Dall'Oglio,<sup>a,b</sup> Marco A. S. Garcia,<sup>b,c</sup> Jhonatan L. Fiorio,<sup>d</sup> Wiury C. de Abreu,<sup>e</sup>  
Laise N. S. Pereira,<sup>f</sup> Adriano Braga,<sup>d</sup> Edmilson M. de Moura,<sup>b,a</sup> Abhishek Guldhe,<sup>g</sup>  
Faizal Bux<sup>b,g</sup> and Carla V. R. de Moura<sup>b\*,a</sup>

<sup>a</sup>Departamento de Química, Universidade Federal do Piauí, 64049-550 Teresina-PI, Brazil

<sup>b</sup>Centro de Ciências Agrárias e Ambientais, Universidade Federal do Maranhão,  
65500-000 Chapadinha-MA, Brazil

<sup>c</sup>Departamento de Química, Universidade Federal do Maranhão, Avenida dos Portugueses, 1966,  
65080-805 São Luís-MA, Brazil

<sup>d</sup>Departamento de Química Fundamental, Universidade de São Paulo, 05508-000 São Paulo-SP, Brazil

<sup>e</sup>Instituto Federal de Educação, Ciência e Tecnologia do Maranhão, 65393-000 Buriticupu-MA, Brazil

<sup>f</sup>Instituto Federal do Maranhão, Campus São Raimundo das Mangabeiras,  
Rodovia BR-230, Km 319, 65840-000 São Raimundo das Mangabeiras-MA, Brazil

<sup>g</sup>Institute for Water and Wastewater Technology, Durban University of Technology,  
PO Box 1334, South Africa

A catalyst comprised of SnO<sub>2</sub> impregnated on ZnO nanowires, which presented remarkable ability to catalyze fatty acid esterification/transesterification reactions, is reported. For optimization of reaction conditions, artificially acidified soybean oil with 10 wt.% oleic acid was used as a model feed. The optimized conditions were: 150 °C, 6 h, 5 g of oil, catalyst concentration of 5%, and methanol:oil molar ratio of 15:1. The catalyst achieved 92% of total fatty acid methyl esters (FAME) content and was used five times without the necessity of catalyst washing from one reaction to the other. Then, such conditions were applied to produce biodiesel from the oil extracted from *Scenedesmus* sp. microalgae; the system reached 72% of FAME content, without any previous refining or degumming process of the oil. Rietveld refinement, X-ray diffraction, elemental mapping in scanning transmission electron microscopy, X-ray photoelectron spectroscopy, and pyridine-desorption Fourier-transform infrared spectroscopy were used to characterize the material.

**Keywords:** acid catalyst, SnO<sub>2</sub>/ZnO, *Scenedesmus* sp. microalgae, biodiesel

### Introduction

The finite natural fossil fuel resources and the necessity of mitigating carbon dioxide emissions are great concerns at the moment.<sup>1</sup> In this context, biodiesel has become more attractive in recent years due to its renewability, less toxicity when compared to petroleum diesel, and environmental appeal since it is free from sulfur, aromatics and produces less soot, carbon oxide, and carbon dioxide.<sup>2</sup> Although the most common raw materials used for biodiesel production are vegetable oils and animal fat,<sup>3</sup> non-edible oils extracted

from microalgal biomass have been lately considered once their production does not need arable lands for cultivation.<sup>4</sup> The use of these substrates is sometimes difficult due to their typical high acid values, which demands the use of acid catalysts.<sup>5</sup> Such reactions are conventionally catalyzed under homogeneous conditions using concentrated sulfuric acid, which is corrosive and dangerous.<sup>6</sup>

Thus, solid acid catalysts are preferable as they eliminate such problems and can be easily separated from the reaction medium by simple filtration. Several solid acid catalysts are described in the literature for long-chain fatty acids esterification reactions, including mesoporous zirconium oxophosphates,<sup>6</sup> zeolites,<sup>7</sup> sulfated

\*e-mail: carla@ufpi.edu.br

zirconia,<sup>7,8</sup> silica zirconia,<sup>9</sup> sulfated zirconium phosphate supported by different metal oxides and mesoporous silica organosulfonic acid.<sup>10,11</sup> Also, strong bifunctional acid catalysts, i.e., with Brønsted and Lewis sites, have received considerable attention due to their synergistic effect, which can effectively improve the catalytic activity of various reactions, such as acetalization, polymerization, benzylation, and oxidation reactions.<sup>12</sup> Pan *et al.*<sup>12</sup> have synthesized a Brønsted-Lewis acid bifunctional catalyst ([1,3-disulfonic acid imidazolium chloride][FeCl<sub>4</sub>]) and used it to prepare biodiesel with 98.7% of conversion to the desired products. Our group has obtained a Brønsted/Lewis acid catalyst from Cr/Al oxide and employed it in the synthesis of babassu oil biodiesel. The system has reached 98.6% of conversion.<sup>13</sup>

Sometimes, harsh conditions, e.g., high temperatures and long reaction times, are necessary for the efficiency of transesterification reactions that use acid catalysts.<sup>14</sup> On the other hand, the use of alkali catalysts can be suitable, considering the milder reaction conditions, but the saponification is a great issue to be solved.<sup>15</sup> Bearing that in mind, some strategies can be designed. For instance, the hydrophobicity that metal oxides present directly affects their performance on the biodiesel synthesis from oils with high acidity value, due to their natural protection against deactivation by the water produced during the reaction.<sup>5</sup> Therefore, choosing the correct mixture of oxides is crucial for the catalysis. Much has been suggested on the field, but sulfonated metal oxides are more frequently used. The process proposes the synthesis of materials that present active acid sites promoted by sulfation.<sup>16</sup> A series of active sulfated metal oxides have been exploited, which includes SO<sub>4</sub><sup>2-</sup>/ZrO<sub>2</sub>,<sup>17,18</sup> SO<sub>4</sub><sup>2-</sup>/TiO<sub>2</sub>,<sup>19</sup> SO<sub>4</sub><sup>2-</sup>/TiO<sub>2</sub>-SiO<sub>2</sub>,<sup>20</sup> SO<sub>4</sub><sup>2-</sup>/ZrO<sub>2</sub>-SiO<sub>2</sub>,<sup>21</sup> SO<sub>4</sub><sup>2-</sup>/TiO<sub>2</sub>-Fe<sub>2</sub>O<sub>3</sub>,<sup>22</sup> SO<sub>4</sub><sup>2-</sup>/SnO<sub>2</sub>,<sup>23</sup> SO<sub>4</sub><sup>2-</sup>/Al<sub>2</sub>O<sub>3</sub>-SnO<sub>2</sub>,<sup>24</sup> and SO<sub>4</sub><sup>2-</sup>/ZnO,<sup>25</sup> among others.<sup>5,25,26</sup> for transesterification and esterification reactions and remarkable results were achieved. However, sulfated catalysts are known to undergo leaching due to the polar medium and the water generated in esterification reactions.<sup>27,28</sup> Thus, to overcome this drawback, the natural acidic properties of the oxides can be explored.

Naked zinc oxide (ZnO) nanomaterials have been successfully applied for biodiesel production. Nambo *et al.*<sup>29</sup> showed their applicability as nanorods in olive oil transesterification, while Archana *et al.*<sup>30</sup> demonstrated their ability as nanoparticles for the biodiesel production from *Aegle marmelos* oil. Also, ZnO presents noteworthy applications as catalytic support for several esterification/transesterification reactions. Baskar and Aiswarya<sup>31</sup> have proposed a heterogeneous catalyst comprised of copper-doped zinc oxide for biodiesel production from waste

cooking oil. Under optimized conditions, the obtained biodiesel conversion was 97.71% with good performance in at least five runs.

Once Brønsted acid catalysts are more active in esterification reactions, and Lewis acid catalysts are more effective for transesterification ones,<sup>32,33</sup> both sites are important when higher quantity of fatty acid are available in oils. Known for some time, the transesterification reaction of soybean oil with methanol performed with some transition metal salts suggests that the strength of Lewis acid sites is: Sn<sup>2+</sup> >> Zn<sup>2+</sup> > Pb<sup>2+</sup> ca. Hg<sup>2+</sup>.<sup>34</sup> Abreu *et al.*<sup>35</sup> have shown the applicability of SnO for biodiesel production of soybean oil. Although the data have not dealt with Sn<sup>4+</sup>, we decided to study such cation for biodiesel production once it is not available in the literature. Thus, attempts to use ZnO and SnO<sub>2</sub> materials as a Brønsted and Lewis acid catalyst are worthy and, to the best of our knowledge, not explored in the literature up to now for biodiesel production. Also, successful examples using SnO<sub>2</sub>/γ-Fe<sub>2</sub>O<sub>3</sub>,<sup>36</sup> mixed iron/tin,<sup>37</sup> SnO<sub>2</sub>/dolomite,<sup>38</sup> (Al<sub>2</sub>O<sub>3</sub>)<sub>8</sub>(SnO)<sub>2</sub>,<sup>39</sup> copper doped zinc oxide,<sup>32</sup> and iron(II) doped zinc oxide<sup>40</sup> as catalysts for biodiesel production are available. We have synthesized ZnO nanowires because the synthesis described in the literature is cost-effective and fast, with a high purity.<sup>41</sup>

Herein, we presented the synthesis of a catalyst comprised of ZnO and SnO<sub>2</sub> for simultaneous esterification and transesterification reactions for biodiesel production. Soybean oil was artificially acidified with 10 wt.% oleic acid to present an acid value compared to the *Scenedesmus* sp. microalgae oil and used to optimize the performance of the catalyst. The material was fully characterized by Rietveld refinement, X-ray photoelectron spectroscopy, elemental mapping in scanning transmission electron microscopy, and pyridine-desorption Fourier-transform infrared spectroscopy.

## Experimental

All reagents were of analytical grade (Sigma-Aldrich, Saint Louis, Missouri, USA) and used without further purification. Refined soybean oil was purchased from a local market (Teresina, PI, Brazil) and used without any degumming procedure. Before the catalytic experiments, the refined soybean oil was acidified under stirring with 10 wt.% oleic acid (isomer not specified by the producer, product number: O1008) by just mixing 10 g of oleic acid with 90 g of soybean oil. The *Scenedesmus* sp. microalgae oil was extracted as previously reported by some of us.<sup>42</sup> Specifically, we used as extraction conditions: CHCl<sub>3</sub>:MeOH (2:1); ultrasound for 2 h, and 60 °C.

### Catalyst preparation

Zinc oxide nanowires were prepared by a previously described method in the literature.<sup>41</sup> The tin has been impregnated in the support (ZnO) using a wet impregnation method. Briefly, 0.5 g of zinc acetate dihydrate ( $\geq 99.0\%$ ) was placed in an alumina crucible and calcined in a muffle furnace for 6 h at 300 °C (heating rate = 20 °C min<sup>-1</sup>). A quantity of SnCl<sub>2</sub>·2H<sub>2</sub>O (98%) was dissolved in ethanol to give 10% of tin on the support, and the mixture was vigorously stirred while the ZnO was added. After 6 h of constant stirring, the solvent was removed under reduced pressure, and the solid was ground to a fine powder; then, washed three times with water. The material was subsequently calcined at 300 °C for 6 h (heating rate = 20 °C min<sup>-1</sup>) and designated as the SnO<sub>2</sub>/ZnO catalyst.

### Catalytic reactions

The reactions were carried out in a 100-mL Teflon-lined stainless-steel autoclave. A heating plate coupled with digital temperature control (Arec X, Velp Scientifica) was used in the experiments. In a typical procedure, catalyst and methanol were mixed in the Teflon liner and stirred during 30 min before the addition of substrate (acidified soybean oil or *Scenedesmus* sp. microalgae oil) at 60 °C. Then, the liner was placed in the autoclave, and the system was positioned in an oil bath, under 600 rpm of stirring. The reaction conditions after optimization were: 5 g of oil, 5% of catalyst (related to the oil mass), 150 °C and methanol to oil molar ratio of 15:1. Any further modifications will be clearly stated in this work. At the end of the reaction, the system was cooled down to room temperature and, after centrifugation, the catalyst was recovered. The resulting mixture of the reaction was placed in a separating funnel and any excess of methanol was drained, and the upper phase was collected (the process was performed three times). Anhydrous sodium sulfate ( $\geq 99.0\%$ ) was used to remove any trace of water before analysis of the products. After the optimization of the catalytic conditions, the catalyst was reused without substantial loss of activity. From one run to the other, no washing procedure was performed, as the best condition. However, two other procedures using ether/ethanol (1:1) and hexane/water + methanol for washing were also tried. From one run to the other, the catalyst was dried in an oven overnight at 100 °C, under static air, in a ceramic container.

### Characterizations

JEOL JEM 2100F transmission electron microscope operating at 200 kV, with a field emission gun and equipped

with an energy dispersive spectrometer (Oxford X-MaxN 100TLE) was used to obtain scanning transmission electron microscopy (STEM) images of the as-prepared and spent catalyst (without washing). The images were acquired on bright-field and high angle-annular dark-field detection with a spot size of 1.5 nm. The element distribution maps were recorded using energy-dispersive X-ray spectroscopy (EDS). Fatty acid methyl esters (FAME) content was determined according to EN 14103,<sup>43</sup> by using gas chromatography (GC, Shimadzu GC-2010) coupled with flame ionization detector (FID) and Rtx-Wax capillary column. At the end of the reaction, the products were transferred for a separating funnel and washed twice with a mixture of 50 mL of distilled water and 25 mL of hexane. The aqueous phase was discarded, and 1  $\mu$ L of the final mixture was injected using a column temperature of 210 °C for 50 min; the temperature of FID was 250 °C and the H<sub>2</sub>, air, and carrier gas (N<sub>2</sub>/air) flows were 40, 400 and 25 mL min<sup>-1</sup>, respectively. The GC-FID chromatogram was used to determine the relative concentrations using peak areas.

X-ray diffraction (XRD) measurements were obtained using a Bruker D8 Advance at a 2 $\theta$  range from 10 to 90° with a 0.02° step size and measuring time of 5 s *per* step. The phases' composition identification was performed by Rietveld refinement using ReX software version 0.8.2.<sup>44</sup> X-ray photoelectron spectroscopy (XPS) data were obtained with ESCA + spectrometer system equipped with an EA 125 hemispherical analyzer and XM 1000 monochromated X-ray source (Scientia Omicron, Uppsala, Sweden) in Al K (1486.7 eV). The calibration was performed using C 1s peak (binding energy, BE = 284.8 eV). Textural characteristics were determined from nitrogen adsorption isotherms, recorded at -196 °C. The samples (100 mg) were degassed for 2 h at 150 °C before analysis. Specific surface area was obtained by the Brunauer-Emmett-Teller equation (BET method) from adsorption isotherm generated in a relative pressure range 0.07 < P/P<sub>0</sub> < 0.3 using Autosorb IQ-Quantachrome Instrument. The metal content in the catalysts (before and after usage) was measured by flame atomic absorption spectroscopy (FAAS), using an AA-6300 atomic absorption spectrophotometer (Shimadzu Corp, Kyoto, Japan). A PerkinElmer spectrum 100 GX FT-IR system set to measure 16 cumulative scans at 4 cm<sup>-1</sup> in a range between 1700 and 1400 cm<sup>-1</sup> was used to obtain Fourier-transform infrared spectroscopy (FTIR) analyses. The acid value of the oils used herein was measured by the D664-07 method.<sup>45</sup> The acid content was calculated by the equation:

$$q_{H,L} = (A\pi D^2)(4w\epsilon)^{-1} \quad (1)$$

where  $D$  (cm) is the diameter of the wafer, and  $w$  (g) the sample weight. The equipment software provided the integrated area  $A$  (in arbitrary units) of the bands at 1515-1565 (Brønsted) and 1435-1470  $\text{cm}^{-1}$  (Lewis). The extinction coefficients  $\epsilon$  of pyridine in interaction with Brønsted and Lewis sites are  $1.67 \pm 0.12$  and  $2.22 \pm 0.21 \text{ cm mmol}^{-1}$ , respectively.<sup>46</sup> In a typical analysis, a sample was heated to 300 °C for 3 h before preparing wafers of approximately 30 mg of catalyst in 100 mg of KBr. Then, an  $\text{N}_2$  flow of 40  $\text{mL min}^{-1}$  went through the sample at 100 °C for 20 min. Next, 1 mbar of pyridine was admitted to the cell. After 1 h of adsorption, the excess and weakly adsorbed pyridine was removed by evacuation at the same temperature for 30 min. The spectra were recorded in the transmission mode. The process was repeated at 200 °C.

## Results and Discussion

### Morphological and structural characteristics

The as-prepared material was characterized to confirm its composition and structure; then, used as a catalyst to check its performance in the transesterification reaction of refined soybean oil acidified with 10 wt.% oleic acid. Such a substrate was used for catalytic optimization before application of the material in the biodiesel production from the oil extracted from *Scenedesmus* sp. microalgae. The  $\text{SnO}_2/\text{ZnO}$  catalyst presented a surface area of 76.3  $\text{m}^2 \text{ g}^{-1}$  (naked ZnO presented surface area of 85.2  $\text{m}^2 \text{ g}^{-1}$ ).

The crystal phases of the catalyst were identified by powder XRD, as we expected to obtain ZnO and  $\text{SnO}_2$  phases. The  $\text{SnO}_2$  would be produced from  $\text{SnCl}_2$  oxidation under heating, and air.<sup>47</sup> Basically, the basic properties of

$\text{SnCl}_2$  are responsible for the oxidation in the presence of  $\text{O}_2$ .  $\text{SnCl}_2$  oxides to  $\text{Sn(OH)Cl}$  under heating (100 °C). Then, tin oxychloride decomposes to  $\text{SnCl}_4$  and  $\text{SnO}_2$  at 120 °C. As we used 300 °C, we believe all the  $\text{SnCl}_4$  becomes  $\text{SnO}_2$ , which was confirmed forward.

Figure 1a shows the patterns of zinc oxide, tin oxide, and the prepared catalyst. The XRD peaks shift towards higher angles observed in the catalyst indicates an improvement in the overall crystal structure. The apparent difficulty of finding  $\text{SnO}_2$  characteristic peaks in the XRD analysis of the catalyst might be related to the formation of an amorphous  $\text{SnO}_2$  phase. Thus, the Rietveld refinement (Figure 1b) was performed to quantify the number of crystalline phases of the catalyst and the presence of  $\text{SnO}_2$ . They were indexed as ZnO (International Crystal Structure Database (ICSD) No. 57450) and  $\text{SnO}_2$  (ICSD No. 160667), resulting in 88.08% of ZnO and 11.92% of  $\text{SnO}_2$ . The ZnO nanoparticles present space group of P63mc (186), with lattice constants  $a = b = 3.1415$  (1) Å, and  $c = 5.033$  (1) Å. The XRD peaks of  $\text{SnO}_2$  can be attributed to the rutile type tetragonal structure, space group of P42/mnm (136), with lattice constants  $a = b = 4.7347$  (1) Å, and  $c = 3.1946$  (1) Å. The quality of the data from structural refinement has been verified by R values related to  $R_{\text{profile}}$  ( $R_p$ ),  $R_{\text{expected}}$  ( $R_{\text{exp}}$ ),  $R_{\text{weighted}}$  ( $R_{\text{wp}}$ ) profiles and the goodness of fit (GoF). More details regarding the Rietveld refinement are shown in Table 1. To measure the quantity of ZnO and  $\text{SnO}_2$  present in the catalyst, we used three different techniques: XRD, FAAS, and EDS. Data are displayed in Table 2 and showed a good agreement among the techniques.

To get further information on the physical characteristics of the  $\text{SnO}_2/\text{ZnO}$  catalyst, the material was analyzed by TEM and STEM images and EDS, which are shown in Figure 2.

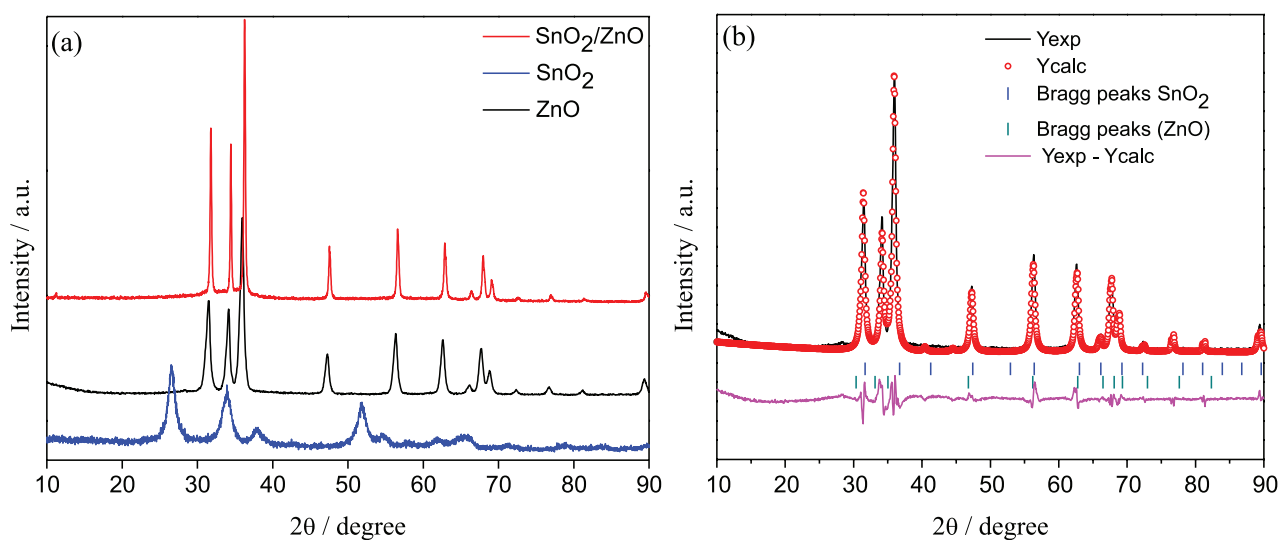


**Figure 1.** (a) XRD patterns of the  $\text{SnO}_2$ , ZnO and catalyst. (b) Rietveld refinement of as-prepared catalyst, showing the observed, calculated, and difference pattern.

**Table 1.** Lattice parameters, unit cell volume, and atomic positions obtained from Rietveld refinements of the SnO<sub>2</sub>/ZnO catalyst

Atom	Wyckoff	Site	x	y	z
Zn1	2b	3m.	1/3	2/2	0
O1	2b	3m	1/3	2/3	0.3821(1)
Sn1	2a	m.mm	0	0	0
O1	4f	m.2m	0.30573(9)	0.30573(9)	0

Phase 1-ZnO: P63 mc (186)-hexagonal ( $a = b = 3.1415$  (1) Å,  $c = 5.033$  (1) Å,  $a/b = 1.0000$ ,  $b/c = 0.6242$ ,  $c/a = 1.6021$ , unit cell volume ( $V$ ) = 43.02 (1) Å<sup>3</sup>, number of formula units in one unit cell ( $Z$ ) = 2; phase 2-SnO<sub>2</sub>: P42/ mmm (136)-tetragonal ( $a = b = 4.7347$  (1) Å,  $c = 3.1946$  (1) Å,  $a/b = 1.0000$ ,  $b/c = 1.4754$ ,  $c/a = 0.6183$ ;  $V = 73.10$  (0) Å<sup>3</sup>,  $Z = 2$ ;  $R_p = 5.63\%$ ;  $R_{exp} = 4.6\%$ ;  $R_{wp} = 10.3\%$ ; goodness of fit ( $S$ ) = 2.23%;  $GoF = 4.97$ .

**Table 2.** Measurements of the amounts of oxides present in the catalyst

Technique	ZnO / (% weight)	SnO <sub>2</sub> / (% weight)
XRD	87.9 <sup>a</sup>	9.9 <sup>a</sup>
FAAS	88.5 ± 0.15	9.0 ± 0.07
EDS	89.6 <sup>a</sup>	9.1 <sup>a</sup>

<sup>a</sup>Measurements are an estimation once the techniques are semi-quantitative. XRD: X-ray diffraction; FAAS: flame atomic absorption spectroscopy; EDS: energy-dispersive X-ray spectroscopy.

Low-magnification TEM images of the as-prepared ZnO and SnO<sub>2</sub>/ZnO catalyst are shown in Figures 2a-2b, which indicated that the samples were comprised of a large number of nanowires (diameter 40-60 nm, length 10-20 μm). The size distribution was found to be well described by a lognormal distribution function, and the narrow size distribution demonstrated the robustness of

this approach for ZnO nanowires synthesis. An important feature to confirm was the efficiency of the immobilization of SnO<sub>2</sub> onto the ZnO surface. Elemental mapping images of Zn Kα1 (brown), O Kα1 (red), and Sn Kα1 (green) elements are shown in Figures 2d-2f, respectively, which presented the nanowire-shaped structure showed before. Interestingly, the signal of Sn attests its uniform disposition along the ZnO nanowires, suggesting that the impregnation performed was very efficient. This result confirms that the nanowires synthesis reached our expectations regarding SnO<sub>2</sub>/ZnO interaction.

### Composition analysis

XPS spectra were performed to determine the chemical composition and the surface oxidation states of the proposed material, as shown in Figure 3. The binding energy peaks of O, Zn, Cl, and Sn were identified in the full range spectrum (Survey), and no peaks of other elements were observed (Figure 3a). As the calcination conditions were rather gentle to eliminate residual Cl ions, XPS analysis showed 7.08% of Cl. One may notice that the existence of Cl ions may enhance the surface acidity of the material, owing to the inductive effect on the neighboring hydroxyl groups. The asymmetric profile observed for O1s (Figure 3b) can be fitted to three sub-peaks by a 70% Gaussian/30% Lorentzian line shape, which indicated the presence of three different oxygen species. The energy peak centered at 530.3 eV matches to lattice oxygen in Sn–O–Sn; the peak located at 531.9 eV corresponds to the

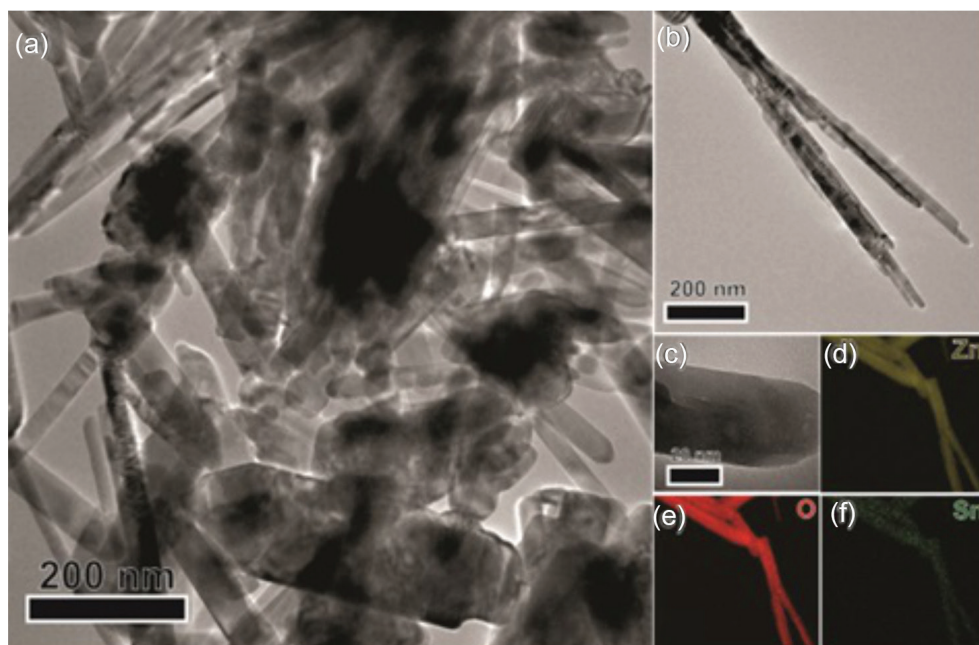


**Figure 2.** Low-magnification TEM images (200 nm) of the as-prepared ZnO nanowires (a) and of the SnO<sub>2</sub>/ZnO material (b). Higher-magnification TEM images (20 nm) of the catalyst (c). Elemental mapping images of Zn Kα1 (d), O Kα1 (e), and Sn Kα1 (f).

O–Zn binding, and the peak at 533.3 eV is attributed to OH species in H<sub>2</sub>O molecules.<sup>48</sup> The high-resolution spectrum for Zn 2p (Figure 3c) presented peaks located at 1021.9 and 1044.9, being attributed to the Zn 2p<sub>3/2</sub> and Zn 2p<sub>1/2</sub> of Zn<sup>2+</sup>, respectively.<sup>49</sup> Figure 3d displays the high-resolution spectrum of tin, in which the peaks located in 487.1 and 495.8 eV are ascribed as Sn 3d<sub>5/2</sub> and Sn 3d<sub>3/2</sub>, respectively, and corresponds to Sn<sup>4+</sup> species.<sup>50</sup> The observed carbon may be attributed to surface hydrocarbon or adventitious hydrocarbons.

### Surface acidity analyses

FTIR spectroscopy was successfully used with pyridine as a basic probe to determine the nature of acid sites on the surface of the material. Figure 4 shows the FTIR spectra of pyridine adsorbed on the catalyst at 100 and 200 °C. The spectra obtained in both temperatures showed sharp pyridine absorption bands around 1445 cm<sup>-1</sup>, which are attributed to the interaction of pyridine with Lewis acid

sites,<sup>51</sup> whereas just discrete signals are observed around 1550 cm<sup>-1</sup> which are due to the protonation of molecules of pyridine by Brønsted acid sites.<sup>52</sup> The weak intensity of peaks for the Brønsted sites suggests that they are in smaller concentrations than the Lewis ones on the material's surface; peaks around 1486 cm<sup>-1</sup> are associated with pyridine molecules adsorbed on both Lewis and Brønsted sites.<sup>53</sup> The peaks around 1608 cm<sup>-1</sup> are also ascribed as the vibration of pyridine molecules adsorbed on Lewis sites,<sup>54</sup> showing its higher quantity when compared to Brønsted sites. Nevertheless, based on equation 1, the Lewis acid contents were 10.5 and 35.43 μmol g<sup>-1</sup> for 100 and 200 °C, respectively, while the Brønsted acid contents were 5.25 and 0.26 μmol g<sup>-1</sup> for 100 and 200 °C, respectively. The total acidity of the catalyst at different temperatures was 15.75 μmol g<sup>-1</sup> for 100 °C and 35.69 μmol g<sup>-1</sup> for 200 °C. Such results are comparable to the acidity of heteropolyacid catalysts, which are considered some of the most acid materials available for catalysis without the necessity of H<sub>2</sub>SO<sub>4</sub> functionalization.<sup>55</sup>

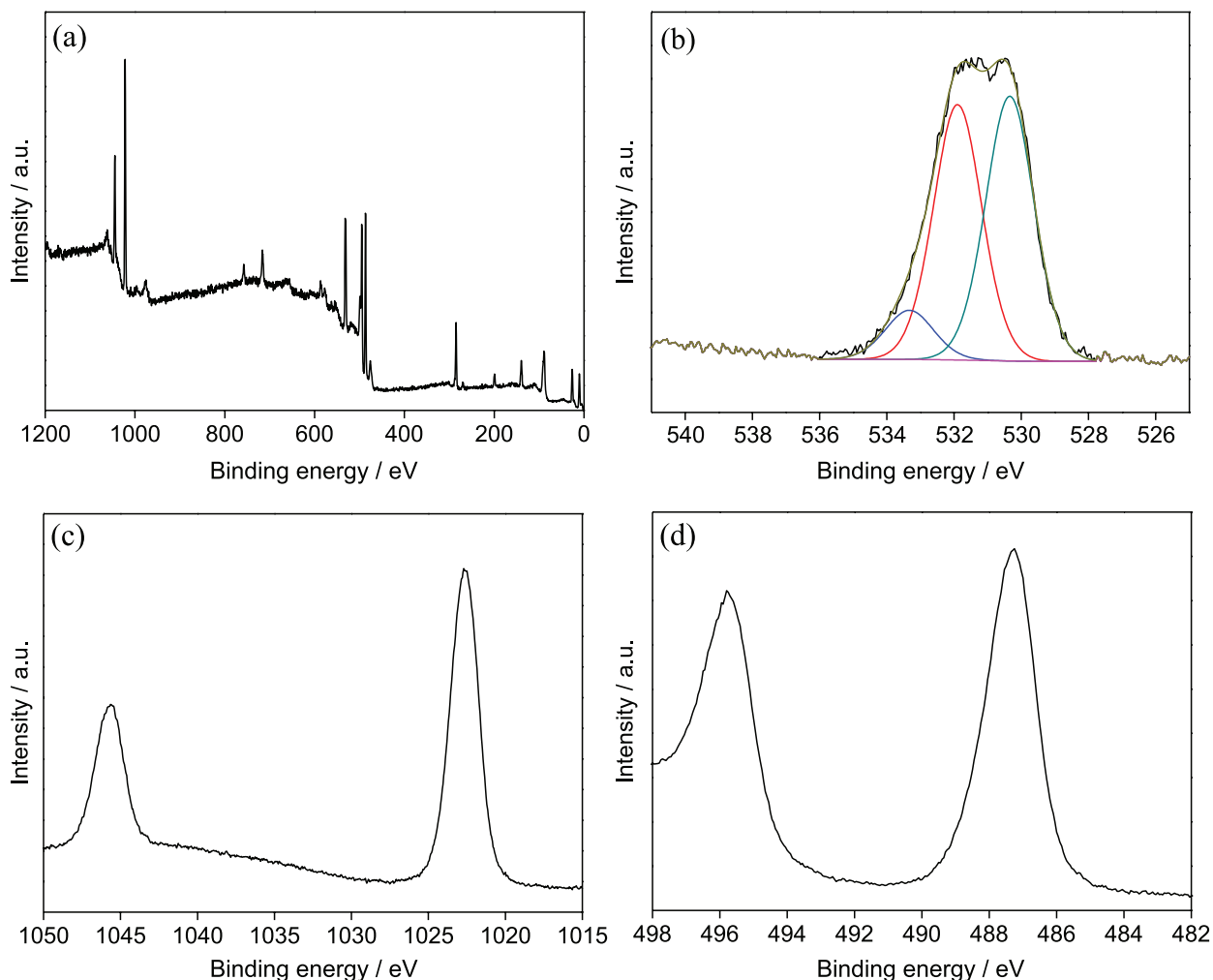


**Figure 3.** XPS spectra of samples SnO<sub>2</sub>/ZnO catalyst. (a) The survey, (b) oxygen, (c) zinc, and (d) tin spectra.

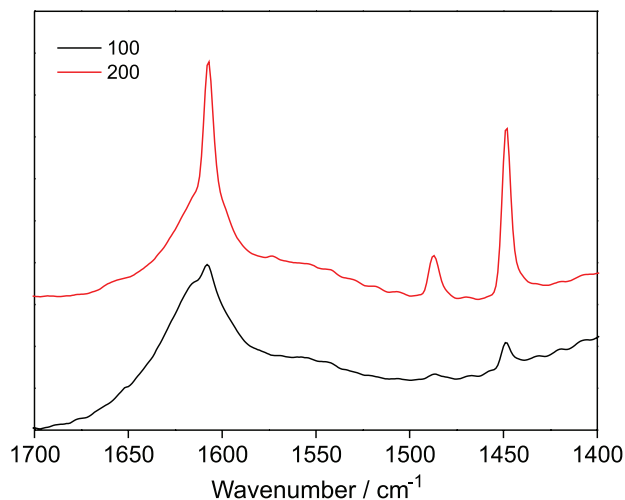


**Figure 4.** FTIR spectra of pyridine adsorbed on SnO<sub>2</sub>/ZnO at 100 and 200 °C.

### Catalytic assessment

The as-synthesized solid material was a very good candidate for biodiesel production due to its properties; acid catalysts present higher tolerance to water and free fatty acids than basic ones, with no soap by-products formation.<sup>14</sup> Also, it presented the possibility of recycling, which improves the net efficiency of the process.<sup>56</sup>

The determined acid value was 20.5 mg KOH g<sup>-1</sup> for *Scenedesmus* sp. microalgae, an indication of the presence of a considerable amount of free fatty acids.<sup>57</sup> According to the literature, Brønsted acid catalysts are more active in esterification reactions, while Lewis acid catalysts are more active for transesterification ones.<sup>31,32</sup> Thus, a catalyst with both acid sites would be suitable. Considering the acidity of the synthesized material, which presents a higher concentration of Lewis sites than Brønsted ones, it is plausible to expect that the SnO<sub>2</sub>/ZnO catalyst presents a higher activity to transesterification reactions; however, the bifunctionality of the material may be an important feature for both reactions. As an initial screening, refined soybean oil (acid value = 0.9 mg KOH g<sup>-1</sup>) and oleic acid underwent reactions for esterification/transesterification, as shown in Table 3. In agreement with the lower concentration of Brønsted acid sites, the FAME content obtained from oleic acid achieved just 47.9%, while the content for the refined soybean oil attained 77.6%, reflecting the higher concentration of Lewis sites.

As far as we can tell, there are no examples in the literature dealing with ZnO nanowires for biodiesel production, nor SnO<sub>2</sub> and SnO by themselves. Also, we decided not to perform ZnO and SnO<sub>2</sub> reactions separately, once some Cl was deposited onto ZnO during the interaction with SnO<sub>2</sub> precursor, which made impossible

the comparison with bare ZnO nanowires. However, the literature presents examples of ZnO mixed with other oxides but rarely deals with only ZnO. Antunes *et al.*<sup>58</sup> used ZnO to produce biodiesel from soybean oil at 100 °C, 7 h, molar ratio of 55:1, and obtained 15% of yield. Kim *et al.*<sup>59</sup> produced simultaneously biodiesel (from rapeseed oil) and ZnO (from zinc nitrate) and presented similar conversion to the obtained here at 250 °C, 5 h, 2.79 g of oil, 4.05 g of methanol, and 400 °C. Although very difficult to make a comparison between our result and the mentioned examples due to obvious differences, our system presents much milder conditions to reach similar performance. Basically, our studies show the viability of using ZnO/SnO<sub>2</sub> as catalysts for biodiesel production.

**Table 3.** FAME content for oleic acid and refined soybean oil<sup>a</sup>

Substrate	FAME content / %
Oleic acid	47.9
Refined soybean oil	77.6

<sup>a</sup>Conditions: 5% of catalyst; oil to alcohol molar ratio: 15:1; 6 h; 150 °C. FAME: fatty acid methyl esters.

Thus, for the optimization experiments, refined soybean oil artificially acidified with 10 wt.% oleic acid was used once its acidity was like that observed for the microalgae oil (21.9 mg KOH g<sup>-1</sup>). We have chosen soybean oil for optimization once the quantity of oil obtained from microalgae is typically low, even under improved conditions.<sup>42</sup>

Thus, the effect of the reaction conditions on the transesterification of the acidified soybean oil was determined by measurements under laboratory conditions. The effect of each variable is described below.

### The effect of temperature

A crucial factor that affects the performance of a catalyst is the reaction temperature since the Lewis and Brønsted sites content changes with the temperature, as stated by the FTIR analyses. For this optimization, seven different reaction temperatures-100, 110, 120, 130, 140, 150, and 160 °C, were selected. For each reaction, the following conditions were considered (15:1 molar ratio, 5% of catalyst, 6 h) and kept constant. According to Figure 5, temperatures below 100 °C would be pointless since at 100 °C the system achieved an exceptionally low conversion (23%). As can be seen, the conversion to ester increased almost linearly with increasing reaction temperature from 100 to 120 °C. Above 120 °C, a discrete augmentation was observed up to 140 °C, attaining the best

conversion at 150 °C (92%). FAME content were 37, 63, 65, and 70% at 110, 120, 130, and 140 °C, respectively. Over 150 °C, the conversion decreased to a value similar to 120 °C (60%). The reason for these phenomena is that the raise of the temperature can reduce the catalyst activity and reverse the reaction since both transesterification and esterification reactions are reversible reactions in nature.<sup>60,61</sup>

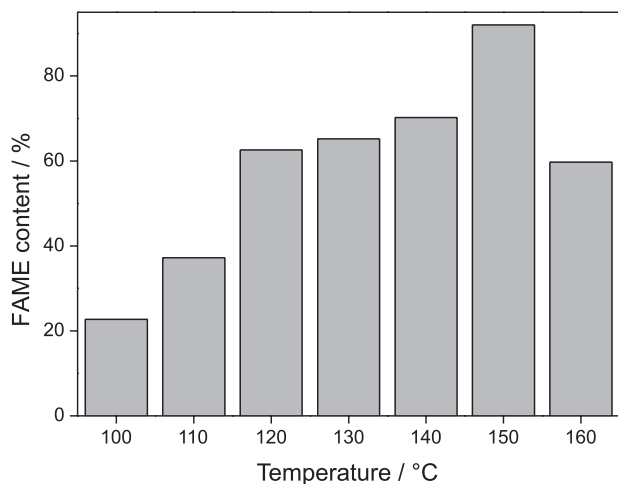


**Figure 5.** Temperature effects on the transesterification of refined acidified soybean oil using the catalyst  $\text{SnO}_2/\text{ZnO}$ . Reaction conditions: 6 h, oil mass = 5 g; catalyst concentration = 5%; methanol:oil molar ratio: 15:1.

#### The effect of catalyst concentration

The effect of the catalyst concentration on the FAME content was the second parameter considered for the optimization of the esterification reaction (Figure 6), as the optimum temperature was set to 150 °C. The reactions were performed using five different catalyst concentrations—1, 3, 5, 7, and 9%—and were carried out by using a 15:1 methanol to oil molar ratio for 6 h at 150 °C. Although the performance of the material was significant with a concentration of 1% of the catalyst (57% of conversion), there was a noteworthy enhancement in the performance from 1 to 5% of  $\text{SnO}_2/\text{ZnO}$  material, i.e., the system reached 92% of FAME content. Further increase in the catalyst concentration gave unsatisfactory FAME content due to mass-transfer restrictions.<sup>62</sup> From the results, the optimum content of biodiesel can be obtained at 5% of catalyst concentration.

#### The effect of molar ratio

Although the literature deals with an excess of methanol for several applications in biodiesel production,<sup>63</sup> one may consider that a large excess of alcohol could slow down the phase separation of the alcohol and biodiesel,<sup>64</sup> and that the purification of the recovered alcohol is difficult

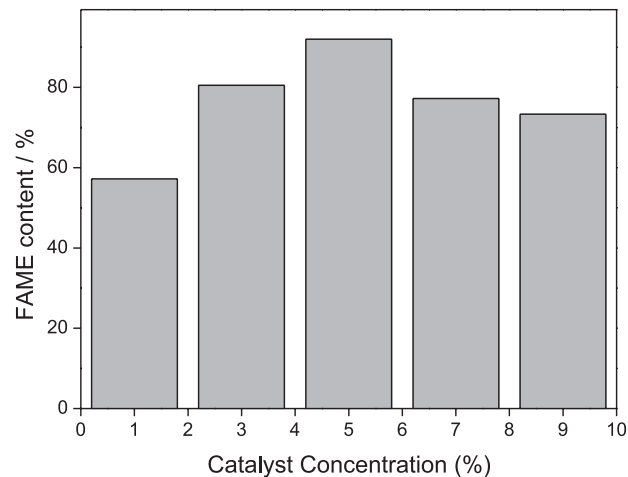


**Figure 6.** Effect of catalyst to oil weight on the transesterification of the refined acidified soybean oil using the  $\text{SnO}_2/\text{ZnO}$  catalyst. Reaction conditions: 150 °C; 6 h; oil mass = 5 g; methanol:oil molar ratio: 15:1.

and costly.<sup>65</sup> Therefore, the molar ratio of methanol to the refined soybean oil is important since it directly influences the conversion of the substrate into the esters.

As shown in Figure 7, a series of reactions were conducted using methanol:oil molar ratios of 6:1, 12:1, 15:1, 18:1, and 30:1 (reaction time of 6 h, temperature of 150 °C, catalyst concentration of 5%). A remarkable enhancement was achieved when the molar ratio was changed from 12:1 to 15:1. However, modifying the molar ratio to 18:1 decreased the conversion, while the molar ratio of 30:1 was highly detrimental for the reaction as the augmentation on the methanol concentration causes a dilution of the oil.<sup>66</sup> Maybe, the excess of methanol, associated to its first addition to the catalyst (and further stirring for 30 min before oil addition) can cause partial blockage of active sites of the catalyst, which provides lower conversion. It

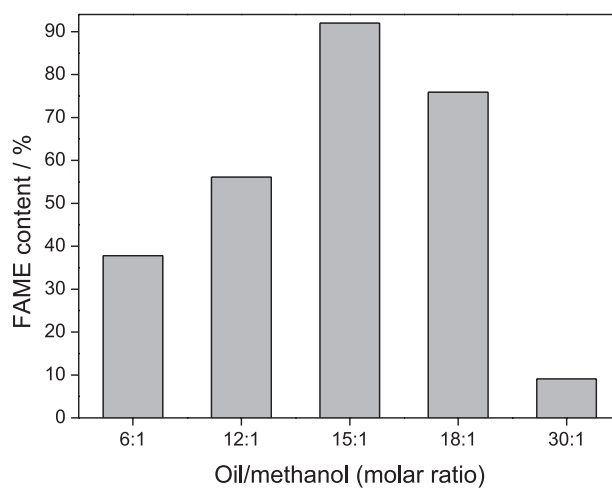


**Figure 7.** Effect of methanol:oil molar ratio on the transesterification reaction of the refined acidified soybean oil using the  $\text{SnO}_2/\text{ZnO}$  catalyst. Reaction conditions: 150 °C; 6 h; oil mass = 5 g; catalyst concentration = 5%.

was quite unexpected since our previously published work with an acid catalyst required at least a molar ratio of 30:1 to present significant conversion.<sup>14</sup> Also, Xie and Wang<sup>67</sup> reported the same molar ratio as the best conditions using tin oxide-supported WO<sub>3</sub> catalysts. Therefore, the molar ratio of 15:1 was the choice for the next optimization step.

#### The effect of reaction time

Five different reaction times—2, 4, 6, 8, and 10 h—were selected for the experiments. For each reaction, the optimized conditions in the previous sections were considered (15:1 molar ratio, 5% of catalyst, at 150 °C) and kept constant. The effect of reaction time on the FAME content is shown in Figure 8. FAME content increased from 77 to 92% when the reaction time was increased from 4 to 6 h. However, long reaction times are detrimental to the system. Such a result suggests that the reaction reached equilibrium, which drove the reverse reaction to occur, i.e., hydrolysis of the biodiesel produced. Thus, considering all the optimization performed herein, tests of recyclability were performed.

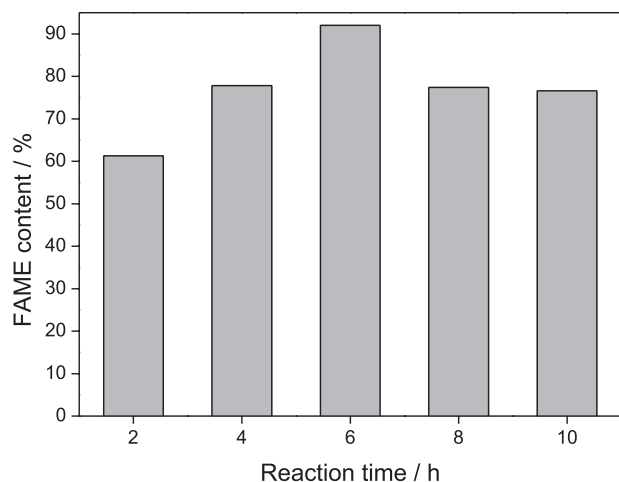


**Figure 8.** Transesterification effects of the refined acidified soybean oil using the catalyst SnO<sub>2</sub>/ZnO catalyst at different reaction times. Reaction conditions: 150 °C; oil mass = 5 g; catalyst concentration = 5%; methanol:oil molar ratio: 15:1.

#### Reusability of the catalyst

Although the catalyst, after the optimization processes, presented a significant activity, recycling experiments were performed once the stability of a system is one of the most important features of a catalyst (Figure 9). In order to evaluate the best procedure for the cleaning of the material after each run, three different washing methods were applied: (i) a mixture of ether and methanol (1:1); (ii) a mixture of hexane and water (1:1) followed by a

methanol washing, and (iii) without washing. All the methods were followed by overnight drying in an oven at 100 °C. The procedure (i) presented a slight increase run in the catalyst performance for the second run; nevertheless, from the third run, the activity reduced linearly up to the fifth run. The procedure (ii) was proposed due to the higher tolerance of solid acid catalysts to water.<sup>68</sup> Also, Interrante *et al.*<sup>69</sup> have shown that a tin(II) oxide heterogeneous catalyst improved its performance when water was added to the reactions system. However, the performance of the catalyst was highly affected in the following cycles. The best results were achieved with procedure (iii). One may notice that this process is within the experimental error, maintaining the performance of the catalyst. Figure 8 shows that the catalyst is very stable up to 5 cycles, with the possibility of more runs, if desirable.

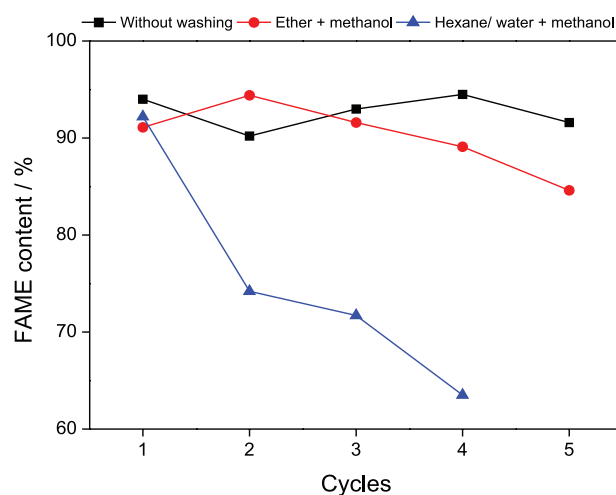


**Figure 9.** Reusability of the SnO<sub>2</sub>/ZnO catalyst for esterification of the refined acidified soybean oil at the optimum reaction conditions. Reaction conditions: 150 °C; 6 h; oil mass = 5 g; catalyst concentration = 5%; methanol:oil molar ratio: 15:1.

After the fifth run, the catalyst was also analyzed by FAAS, and no leaching of Zn or Sn was detected under the limit of detection of the equipment, i.e., the material maintained 9.0 wt.% Sn after five cycles. However, one may notice that after the runs (five in total), there was some damage to the nanowires, as seen in Figures 10a-10e. The modification of the particles surface is probably due to a limited leaching of Zn species, followed by re-deposition once the acid content in the reacting medium becomes low enough to allow the process.

#### Catalytic application on the *Scenedesmus* sp. microalgae

Oil from *Scenedesmus* sp. microalgae was extracted according to Dall'Oglio *et al.*<sup>42</sup> and then, used as a substrate for biodiesel production. The optimized conditions for the

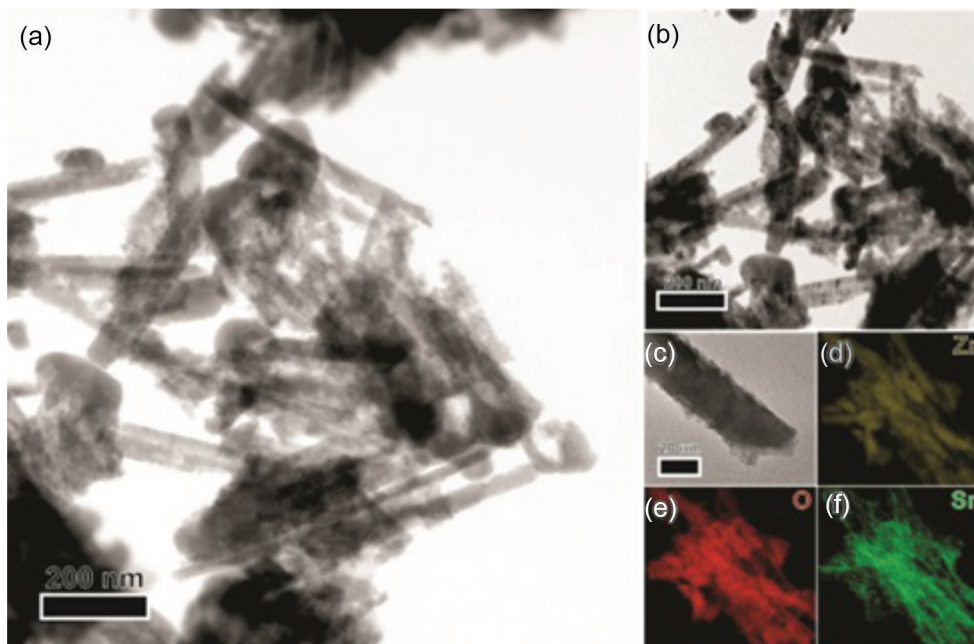


**Figure 10.** Low-magnification TEM images (200 nm) of the as-prepared ZnO nanowires (a) and of the SnO<sub>2</sub>/ZnO material after the fifth run (b). Higher-magnification TEM images (20 nm) of the used catalyst (c). Elemental mapping images of Zn Kα1 (d), O Kα1 (e), and Sn Kα1 (f).

acidified soybean oil were also used for the *Scenedesmus* sp. oil esterification/transesterification. Considering the oil did not undergo any refining or degumming process, the obtained FAME content was quite significant, i.e., reached 72%. One can be aware that the composition of FAME from acidified soybean oil is different from the obtained from a microalgae oil. The reason for that is the middle-chain length fatty acids that are in the mixture, as well as the nitrogen compounds, which can be detrimental to the final product.

## Conclusions

In summary, ZnO nanowires impregnated with SnO<sub>2</sub>, containing Brønsted and Lewis acid sites, were synthesized through thermal treatment of zinc acetate dehydrate, followed by immobilization with SnCl<sub>2</sub>·2H<sub>2</sub>O before calcination at 300 °C. We were able to synthesize a catalyst with both acid sites without the need of sulfation. Pyridine-desorption FTIR spectroscopy confirmed the presence of the acid sites. The nature of the catalyst was analyzed by Rietveld refinement analysis and scanning TEM elemental mappings and XPS spectra. Refined soybean oil acidified with 10 wt.% oleic acid was the substrate used for the optimization of the reaction conditions, which were used in the production of biodiesel from *Scenedesmus* sp. microalgae. The SnO<sub>2</sub>/ZnO material was able to simultaneously catalyze esterification and transesterification reactions. Thus, a 92% FAME content was obtained at 150 °C, using 5 wt.% of catalyst in 6 h of

reaction using the acidified soybean oil. Also, the catalyst was used up to five times without significant performance loss. When the catalyst was applied to the oil extracted from the microalgae, the process reached 72%, which was a very significant result since the oil did not undergo any refining or degumming process. Further studies are needed on the oil extraction and pre-treatment methods opening up the possibility of preparing biodiesel from microalgae using this novel catalyst.

## Acknowledgments

The authors acknowledge financial support from CAPES, CNPq, and the technical support of the Center for Strategic Technology of the Northeast (CETENE-PE). We also thank Dr Liane M. Rossi for the FAAS equipment disponibility. Thanks to CCMC/CDMF (FAPESP No. 2013/07296-2, Brazil) and Prof Dr Renato Vitalino Gonçalves for the XPS measurements.

## Author Contributions

Daiane F. Dall'Oglio was responsible for conceptualization, data curation, methodology, writing-original draft, writing-review and editing; Marco A. S. Garcia for conceptualization, data curation, visualization, writing-original draft, writing-review and editing; Jhonatan L. Fiorio for methodology; Wiury C. de Abreu for data curation; Laise N. S. Pereira for data curation; Adriano Braga for data curation; Edmilson M. de Moura

for conceptualization, funding acquisition, resources, supervision; Abhishek Guldhe for conceptualization, writing-original draft, writing-review and editing; Faizal Bux for conceptualization, funding acquisition, writing-original draft, writing-review and editing; Carla V. R. de Moura for conceptualization, data curation, funding acquisition, project administration, resources, supervision, validation, writing-original draft, writing-review and editing.

## References

- Walsh, B.; Ciaias, P.; Janssens, I. A.; Penuelas, J.; Riahi, K.; Ryzak, F.; Vuuren, D. P. V.; Obersteiner, M.; *Nat. Commun.* **2017**, *8*, 14856.
- Mishra, V. K.; Goswami, R.; *Biofuel* **2018**, *9*, 273.
- Zhang, H.; Li, H.; Pan, H.; Wang, A.; Souzanchi, S.; Xu, C. C.; Yang, S.; *Appl. Energy* **2018**, *223*, 416.
- Randrianarison, G.; Ashraf, M. A.; *Geol. Ecol. Landscapes* **2017**, *1*, 104.
- Thangaraj, B.; Solomon, P. R.; Muniyandi, B.; Ranganathan, S.; Lin, L.; *Clean Energy* **2018**, *3*, 2.
- Das, S. K.; Bhunia, M. K.; Sinha, A. K.; Bhaumik, A.; *ACS Catal.* **2011**, *1*, 493.
- Kiss, A. A.; Dimian, A. C.; Rothenberg, G.; *Adv. Synth. Catal.* **2006**, *348*, 75.
- Kiss, A. A.; Dimian, A. C.; Rothenberg, G.; *Energy Fuels* **2008**, *22*, 598.
- Rosenberg, D. J.; Bachiller-Baeza, B.; Dines, T. J.; Anderson, J. A.; *J. Phys. Chem. B* **2003**, *107*, 6526.
- Rao, K. N.; Sridhar, A.; Lee, A. F.; Tavener, S. J.; Young, N. A.; Wilson, K.; *Green Chem.* **2006**, *8*, 790.
- Zhang, J.; Zou, H.; Qing, Q.; Yang, Y.; Li, Q.; Liu, Z.; Guo, X.; Du, Z.; *J. Phys. Chem. B* **2003**, *107*, 3712.
- Pan, H.; Li, H.; Zhang, H.; Wang, A.; Jin, D.; Yang, S.; *Energy Convers. Manage.* **2018**, *166*, 534.
- Moura, C. V. R.; Neres, H. L. S.; Lima, M. G.; Moura, E. M.; Moita Neto, J. M.; de Oliveira, J. E.; Lima, J. R. O.; Sttolin, I. M.; Araújo, E. C.; *J. Braz. Chem. Soc.* **2016**, *27*, 515.
- Wang, J.; Dong, S.; Yu, C.; Han, X.; Guo, J.; Sun, J.; *Catal. Commun.* **2017**, *92*, 100.
- Pinto, B. F.; Garcia, M. A. S.; Costa, J. C. S.; de Moura, C. V. R.; Abreu, W. C.; de Moura, E. M.; *Fuel* **2019**, *239*, 290.
- Arata, K.; *Green Chem.* **2009**, *11*, 1719.
- Guo-liang, S.; Feng, Y.; Xiao-liang, Y.; Rui-feng, L.; *J. Fuel Chem. Technol.* **2017**, *45*, 311.
- Luo, Y.; Mei, Z.; Liu, N.; Wang, H.; Han, C.; He, S.; *Catal. Today* **2017**, *298*, 99.
- Hosseini-Sarvari, M.; Sodagar, E.; *C. R. Chim.* **2013**, *16*, 229.
- Shao, G. N.; Sheikh, R.; Hilonga, A.; Lee, J. E.; Park, Y.; Kim, H. T.; *Chem. Eng. J.* **2013**, *215*, 600.
- Thitsartarn, W.; Kawi, S.; *Ind. Eng. Chem. Res.* **2011**, *50*, 7857.
- Anuradha, S.; Raj, K. J. A.; Vijayaraghavan, V. R.; Viswanathan, B.; *Indian J. Chem.* **2014**, *53*, 1493.
- Lam, M. K.; Lee, K. T.; Mohamed, A. R.; *Appl. Catal., B* **2009**, *93*, 134.
- Nuithitikul, K.; Prasitturattanachai, W.; *Int. J. Green Energy* **2014**, *11*, 1097.
- Istadi, I.; Anggoro, D. D.; Buchori, L.; Rahmawati, D. A.; Intaningrum, D.; *Procedia Environ. Sci.* **2015**, *23*, 385.
- Guan, Q.; Li, Y.; Chen, Y.; Shi, Y.; Gu, J.; Li, B.; Miao, R.; Chen, Q.; Ning, P.; *RSC Adv.* **2017**, *7*, 7250.
- Sani, Y. M.; Daud, W. M. A. W.; Aziz, A. R. A.; *Appl. Catal., A* **2014**, *470*, 140.
- Diamantopoulos, N.; Panagiotaras, D.; Nikolopoulos, D.; *J. Thermodyn. Catal.* **2015**, *6*, 143.
- Nambo, A.; Miralda, C. M.; Jasinski, J. B.; Carreon, M. A.; *React. Kinet., Mech. Catal.* **2015**, *114*, 583.
- Archana, B.; Nagaraju, G.; Yatish, K. V.; Udayabhanu; Sekhar, K. B. C.; Kottam, N.; *AIP Conf. Proc.* **2018**, *1992*, 030004.
- Baskar, G.; Aiswarya, R.; *Bioresour. Technol.* **2015**, *188*, 124.
- di Serio, M.; Tesser, R.; Dimiccoli, M.; Cammarota, F.; Nastasi, M.; Santacesaria, E.; *J. Mol. Catal. A: Chem.* **2005**, *239*, 111.
- Su, F.; Guo, Y.; *Green Chem.* **2014**, *16*, 2934.
- Abreu, F. R.; Lima, D. G.; Hamú, E. H.; Einloft, S.; Rubim, J. C.; Suarez, P. A. Z.; *J. Am. Oil Chem. Soc.* **2003**, *80*, 601.
- Abreu, F. R.; Alves, M. B.; Macêdo, C. C. S.; Zara, L. F.; Suarez, P. A. Z.; *J. Mol. Catal. A: Chem.* **2005**, *227*, 263.
- Akkarawatkhoosith, N.; Jaree, A.; *Appl. Surf. Sci.* **2018**, *456*, 615.
- Alves, M. B.; Medeiros, F. C. M.; Sousa, M. H.; Rubim, J. C.; Suarez, P. A. Z.; *J. Braz. Chem. Soc.* **2014**, *25*, 2304.
- Shajaratun Nur, Z. A.; Taufiq-Yap, Y. H.; Nizah, M. F. R.; Teo, S. H.; Syazwani, O. N. S.; Islam, A.; *Energy Convers. Manage.* **2014**, *78*, 738.
- Mello, V. M.; Pousa, G. P. A. G.; Pereira, M. S. C.; Dias, I. M.; Suarez, P. A. Z.; *Fuel Process. Technol.* **2011**, *92*, 53.
- Baskar, G.; Soumiya, S.; *Renewable Energy* **2016**, *98*, 101.
- Lin, C.; Li, Y.; *Mater. Chem. Phys.* **2009**, *113*, 334.
- Dall'Oglio, D. F.; de Sousa, L. C.; de Sousa, S. A. A.; Garcia, M. A. S.; Sousa, E. S.; de Lima, S. G.; Costa, P. S.; Guldhe, A.; Bux, F.; de Moura, E. M.; de Moura, C. V. R.; *J. Braz. Chem. Soc.* **2019**, *30*, 633.
- EN 14103:2003: *Fatty Acid Methyl Esters (FAME), Determination of Ester and Linolenic Acid Methyl Esters Contents*, European Committee for Standardization, Brussels, 2003.
- ReX Powder Diffraction Analysis Software*, version 0.8.2; ReXpd Software Ltd., USA, 2016.
- ASTM D664-18e2: *Standard Test Method for Acid Number of Petroleum Products by Potentiometric Titration*, West Conshohocken, PA, 2018.

46. Emeis, C. A.; *J. Catal.* **1993**, *141*, 347.
47. Butem, R.; Kraisingdecha, P.; Sadee, W. In *Fluoride and Antimony-Doped Tin Oxide Film by Spray Pyrolysis*; Tunkasiri, T., ed.; Trans Tech Publications: Zürich, Switzerland, 2008.
48. Li, C. C.; Yin, X. M.; Li, Q. H.; Wang, T. H.; *CrystEngComm* **2011**, *13*, 1557.
49. Balachandran, S.; Selvam, K.; Babu, B.; Swaminathan, M.; *Dalton Trans.* **2013**, *42*, 16365.
50. Wang, L.; Li, J.; Wang, Y.; Yu, K.; Tang, X.; Zhang, Y.; Wang, S.; Wei, C.; *Sci. Rep.* **2016**, *6*, 35079.
51. Yazici, D. T.; Bilgiç, C.; *Surf. Interface Anal.* **2010**, *42*, 959.
52. Morterra, C.; Cerrato, G.; Pinna, F.; Meligrana, G.; *Top. Catal.* **2001**, *15*, 53.
53. El-sayed, Y.; Abu-farha, N.; Kanan, S.; *Vib. Spectrosc.* **2014**, *75*, 78.
54. Rabee, A. I. M.; Mekhemer, G. A. H.; Osatiashtiani, A.; Isaacs, M. A.; Lee, A. F.; Wilson, K.; Zaki, M. I.; *Catalysts* **2017**, *7*, 204.
55. Tao, M.; Xue, L.; Sun, Z.; Wang, S.; Wang, X.; Shi, J.; *Sci. Rep.* **2015**, *5*, 13764.
56. Sheikh, R.; Choi, M.; Im, J.; Park, Y.; *J. Ind. Eng. Chem.* **2013**, *19*, 1413.
57. Guldhe, A.; Singh, B.; Rawat, I.; Bux, F.; *Chem. Eng. Res. Des.* **2014**, *92*, 1503.
58. Antunes, W. M.; Veloso, C. O.; Henriques, C. A.; *Catal. Today* **2008**, *133*, 548.
59. Kim, M.; Lee, H.-S.; Yoo, S. J.; Youn, Y.-S.; Shin, Y. H.; Lee, Y.-W.; *Fuel* **2013**, *109*, 279.
60. Anbessa, T. T.; Karthikeyan, S.; *Int. J. Eng. Adv. Technol.* **2019**, *9*, 1733.
61. Srilatha, K.; Lingaiah, N.; Devi, B. L. A. P.; Prasad, R. B. N.; Venkateswar, S.; Prasad, P. S. S.; *Appl. Catal., A* **2009**, *365*, 28.
62. Bhoi, R.; Singh, D.; Mahajani, S.; *React. Chem. Eng.* **2017**, *2*, 740.
63. Lee, A. F.; Bennett, J. A.; Manayil, J. C.; Wilson, K.; *Chem. Soc. Rev.* **2014**, *43*, 7887.
64. Antolín, G.; Tinaut, F. V.; Briceno, Y.; Pérez, C.; Ramírez, A. I.; *Bioresour. Technol.* **2002**, *83*, 111.
65. Behzadi, S.; Farid, M. M.; *Bioresour. Technol.* **2009**, *100*, 683.
66. Takase, M.; Chen, Y.; Liu, H.; Zhao, T.; Yang, L.; Wu, X.; *Ultrason. Sonochem.* **2014**, *21*, 1752.
67. Xie, W.; Wang, T.; *Fuel Process. Technol.* **2013**, *109*, 150.
68. Tran, H. L.; Ryu, Y. J.; Seong, D. H.; Lim, S. M.; Lee, C. G.; *Biotechnol. Bioprocess Eng.* **2013**, *18*, 242.
69. Interrante, L.; Bensaid, S.; Galletti, C.; Pirone, R.; Schiavo, B.; Scialdone, O.; Galia, A.; *Fuel Process. Technol.* **2018**, *177*, 336.

Submitted: January 21, 2020

Published online: August 17, 2020

